AIAA 2001-1238
Probabilistic and Possibilistic Analyses of the Strength of a Bonded Joint

W. Jefferson Stroud, T. Krishnamurthy and
Steven A. Smith
NASA Langley Research Center
Hampton, VA

42nd AIAA/ASME/ASCE/AHS/ASC
Structures, Structural Dynamics, and Materials Conference
16–19 April 2001
Seattle, WA

AIAA-2001-1238

PROBABILISTIC AND POSSIBILISTIC ANALYSES OF THE STRENGTH OF A BONDED JOINT

W. Jefferson Stroud* and T. Krishnamurthy*
NASA Langley Research Center
Hampton, VA 23681-2199

and

Steven A. Smith†
Vehicle Technology Directorate - Army Research Laboratory
NASA Langley Research Center
Hampton, VA 23681-2199

Abstract

The effects of uncertainties on the strength of a single lap shear joint are explained. Probabilistic and possibilistic methods are used to account for uncertainties. Linear and geometrically nonlinear finite element analyses are used in the studies. To evaluate the strength of the joint, fracture in the adhesive and material strength failure in the strap are considered. The study shows that linear analyses yield conservative predictions for failure loads. The possibilistic approach for treating uncertainties appears to be viable for preliminary design, but with several qualifications.

Introduction

In the final stages of the design of future advanced aerospace vehicles, the design procedures need to account for uncertainties by calculating the risk or reliability. These calculations will involve probabilistic analysis. While probabilistic methods may be required in the final stages of design, methods that merely bound a response quantity and provide the most likely value may be adequate for early stages of design. Such methods, referred to herein as possibilistic methods, have the potential for allowing a large number of design options to be evaluated rapidly during the conceptual and preliminary design stages when there may be little data and little need for precision.

When compared with traditional factor-of-safety methods, both probabilistic and possibilistic methods require additional inputs but provide more and higher quality outputs. Variables in these methods can be classified as either certain or uncertain. For probabilistic methods, the uncertain variables are assumed to have a probability density function. In turn, probabilistic methods provide a probability density function for the response quantities. Similarly, possibilistic methods require a membership function for the uncertain parameters, and they provide a membership function for the response quantities.

The general objective of this paper is to study the differences between probabilistic and possibilistic methods by exploring their application to a simple and yet commonly encountered structural component. The selected component is a single lap shear joint. The specific objective of the paper is to study how uncertainties affect the strength of a single lap shear joint. The study considers two ways to account for uncertainties (probabilistic and possibilistic), examines the effect of a geometrically nonlinear analysis, shows the effect of two failure modes (fracture in the adhesive and material strength failure in the strap), and illustrates several computational techniques.

Description of Problem

The single lap shear joint consists of lap and strap adherends bonded with an adhesive as shown in Figure 1. This configuration has been analyzed extensively in References 1-5. The strap is subjected to a tensile load F that is reacted at the x=0 plane. The adhesive is assumed to contain a crack of length c situated centrally within the adhesive. Boundary conditions at the left end of the joint are $u(0,y) = 0$ and $v(0,0) = 0$. These boundary conditions represent

*Aerospace Engineer, Analytical and Computational Methods Branch, Senior Member, AIAA

†Aerospace Engineer, Analytical and Computational Methods Branch, Member AIAA

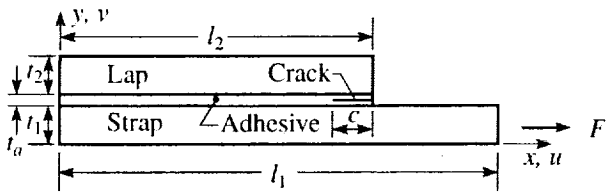

Figure 1 Single lap shear joint.

symmetry conditions. Boundary conditions at the right end of the strap are $u(l_1,y)$ = constant and $v(l_1,0) = 0$. These boundary conditions correspond to zero rotation of the face of the strap at the right end and approximate the restraints provided by the grips in a testing machine. Various configurational and material properties that define the single lap shear joint analyzed in this paper are given in Table 1. The lap and strap adherends are taken to be 2024 T3 aluminum.

The ABAQUS finite element structural analysis program (Ref. 6) was used to analyze the joint. The two-dimensional finite element model of the joint (Fig. 2) had 1692 plane strain, 8-node, biquadratic elements (denoted CPE8) with 5331 nodes. These CPE8 elements were used throughout the model, including at and near the crack tip. Near the crack tip, fine mesh modeling is used (Fig. 2(c)), and equal size elements with aspect ratios 1 are maintained on either side of the crack tip to facilitate strain energy release rate calculations. Linear and geometrically nonlinear analyses were carried out. The nonlinear analysis was carried out to study the effects of eccentricity of the loading and the resulting rotation of the joint.

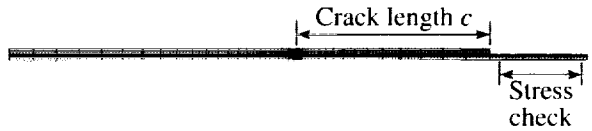

a) Overall model

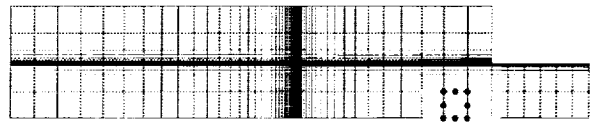

b) Overall model with thickness enlarged to show finite element mesh

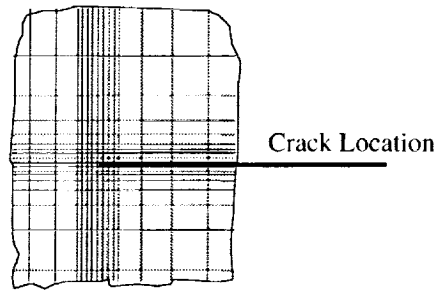

c) Detail near the crack tip

Figure 2. Finite element model of single lap shear joint.

Table 1. Values of quantities that define the single lap shear joint

Variable	Symbol	Probabilistic Analysis (normal distributions)		Possibilistic Analysis α=0	
		Mean	Standard Deviation	Lower Bound	Upper Bound
Thickness, strap – in.	t_1	0.125	0.005	0.11	0.14
Thickness, lap – in.	t_2	0.125	0.005	0.11	0.14
Length, strap – in.	l_1	12.0	0	12	12
Length, lap – in.	l_2	10.0	0.16	9.52	10.48
Thickness, adhesive – in.	t_a	0.0050	0.0005	0.0035	0.0065
Length, crack – in.	c	4.00	0.08	3.76	4.24
Modulus, metallic adherends - psi	E_m	10,500,000	105,000	10,185,000	10,815,000
Poisson's ratio, metallic adherends	ν_m	0.3125	0	0.3125	0.3125
Modulus, adhesive - psi	E_a	336,000	16,800	285,600	386,400
Poisson's ratio, adhesive	ν_a	0.40	0	0.4	0.4
Critical value of G (total) – in. lb/in.^{2}	G_c	5.50	0.66	3.52	7.48
Yield stress 2024 T3 - psi	σ_{yield}	44,000	880	41,360	46,640
Crack Growth Increment – in.	Δc	0.00125	0	0.00125	0.00125

To study the effect of uncertainties, nine of the quantities in Table 1 were taken to be independent random variables with normal distributions and with specified means and standard deviations. Two failure modes were considered – fracture in the adhesive due to an existing crack and material strength failure due to yielding in the strap.

Analysis Approach

This section describes the two approaches that were used to treat uncertainty and the two approaches that were used to evaluate failure. Probabilistic and possibilistic approaches were used to treat uncertainty. The two failure modes that were used are fracture in the adhesive caused by an existing crack and material strength failure caused by yield in the strap.

Accounting for Uncertainties

In the probabilistic approach for accounting for uncertainties, nine quantities were assumed to be random variables with normal distributions. The random variables and their statistics are given in Table 1. With these nine random variables, Monte Carlo simulations (Refs. 7, 8) were used to calculate the probability of failure of the joint for various values of the load F. (A brief description of the Monte Carlo method is given in Appendix A.) Convergence of the Monte Carlo calculations was evaluated by using 100, 1000, and 5000 trials and by comparing results from a Monte Carlo simulation with results from a first order reliability method (FORM, Ref. 7). The probabilistic analysis code ProFES (Ref. 9) was used for all these calculations.

In the possibilistic approach (Refs. 10, 11), membership functions were assigned to the nine random variables indicated in Table 1. An example of a membership function is shown in Figure 3. The parameter α indicates the possibility of an uncertain quantity taking on a given value. The objective is to use the membership functions of the input parameters (e.g., dimensions) to determine the corresponding membership functions for the response quantities (e.g., stress, buckling load). Techniques for calculating with membership functions are given in Reference 10. The membership functions for the response quantities are then compared with the membership functions of the allowable responses to determine the possibility of failure. In this paper, the membership functions for the nine random variables are taken to be isosceles triangles with the most likely value (MLV in Fig. 3) equal to the mean value given in Table 1. The most likely value corresponds to $\alpha = 1.0$. The absolute upper and lower bounds (UB and LB in Fig. 3) are equal to the mean value plus/minus three standard deviations. The absolute upper and lower bounds correspond to $\alpha = 0.0$. A brief discussion of membership functions together with an example that illustrates techniques for calculating with membership functions are presented in Appendix B. Comparisons between probabilistic and possibilistic methods are given in Reference 11.

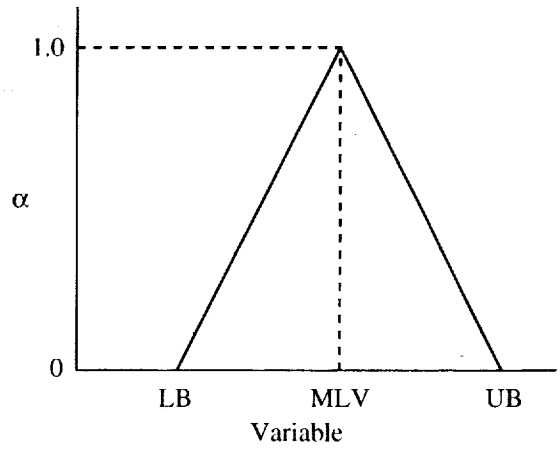

Figure 3. Example of membership function.

Fracture in the Adhesive

The strain energy release rates for self-similar crack growth are used to evaluate fracture in the adhesive due to an existing crack. The evaluation consists of calculating values of the total strain energy release rate G_T and comparing these values with the experimentally determined value of the critical strain energy release rate G_C (Refs. 17, 18). Failure is assumed to occur when the total strain energy release rate is equal to or greater than the critical strain energy release rate, i.e.,

$$G_T \geq G_C \tag{1}$$

For this joint configuration, the total strain energy release rate G_T is given by

$$G_T = G_I + G_{II} \tag{2}$$

where G_I and G_{II} are the strain energy release rates for mode-*I* and mode-*II* failures, respectively. The critical energy release rate in equation (1) for mixed-mode fracture is dependant on the mode-mixity (Refs. 17,

18). The critical energy release rate used in this paper is for FM-300 adhesive tested in mixed-mode conditions with a mode-mixity, $G_I / G_{II} = 0.3$ (Ref. 5).

The "virtual crack closure technique" (VCCT) is used to evaluate G_I and G_{II} using the crack tip forces and the opening and sliding displacements of the crack faces (Refs. 12-16). Due to large rotations of the model in the vicinity of the crack tip, a nonlinear formulation of the VCCT that utilizes a local x'-y' system (see Fig. 4) is used (Refs. 2, 15). The displacements of the crack-tip node and the node ahead of the crack tip are used to determine a local x' axis of the rotated coordinate system. The expressions for G_I and G_{II} in the local coordinate system can be written using the notation shown in figure 4 as:

$$G_I = -\frac{1}{2\Delta c}\left[Y_i'\left(v_m' - v_{m^*}'\right) + Y_j'\left(v_l' - v_{l^*}'\right)\right] \qquad (3)$$

$$G_{II} = -\frac{1}{2\Delta c}\left[X_i'\left(u_m' - u_{m^*}'\right) + X_j'\left(u_l' - u_{l^*}'\right)\right] \qquad (4)$$

where

Δc is the crack growth increment, and is equal to the width of the elements at the crack tip,

X_i, Y_i are the nodal forces at node i evaluated using the elements I and J in the x' and y' directions respectively,

X_j', Y_j' are the nodal forces at node j evaluated using the element I in the x' and y' directions respectively,

$u_m', u_{m^*}', u_l', u_{l^*}'$ are displacements in the x' direction at nodes m, m^*, l, and l^* respectively, and

$v_m', v_{m^*}', v_l', v_{l^*}'$ are displacements in the y' direction at nodes m, m^*, l, and l^* respectively.

The values of the forces and displacements on the right hand sides of equations (3) and (4) are extracted from a finite element analysis.

Material Strength Failure in the Strap

Failure in the strap is assumed to occur when the stress in the strap exceeds the yield stress of the material. The stress was examined in the region denoted "Stress Check" in Figure 2. That region does not include the loaded end, where the boundary conditions may cause local stress perturbations. In the region examined for stress failure, the bending stress is small compared with the extensional stress. (For example, by using a geometrically nonlinear finite element analysis it was determined that the bending stress is less than 1% of the extensional stress at $x = 10$ in., less than 2% at $x = 11$ in., and less than 6% at $x = 11.5$ in. The load F is applied at $x = 12$ in.) Therefore, after setting to unity the depth of the strap, the stress σ_x is taken to be

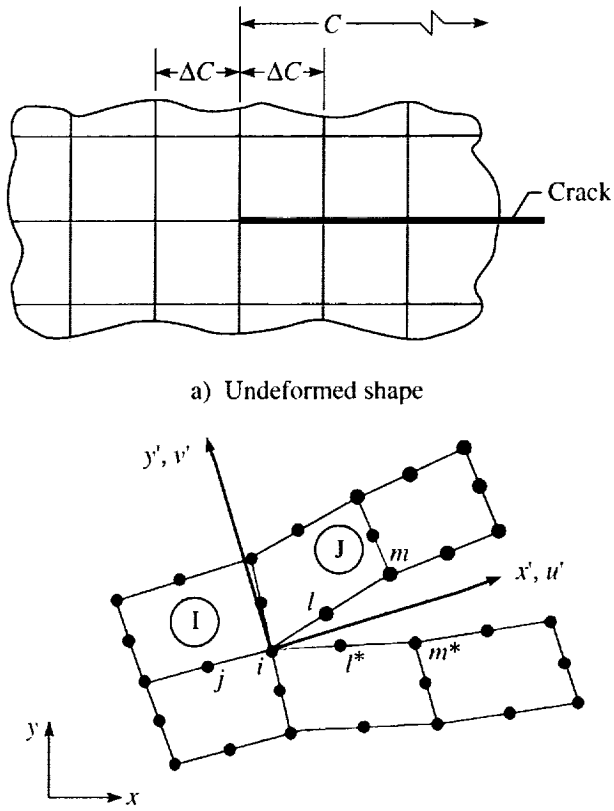

Figure 4. Model and notation used in virtual crack closure technique.

$$\sigma_x = \frac{F}{t_1} \qquad (5)$$

Note that the calculation of σ_x does not require a finite element analysis.

Results and Discussion

Results of deterministic analyses obtained using the mean values of the variables are presented first. Then, results showing the effects of uncertainties are presented.

Deterministic Analyses

The deformed shape of the finite element model for a load of 6000 lb is shown in Figure 5. In the figure, deflections are scaled up by a factor of 10 for visualization purposes. The joint undergoes significant bending.

Figure 5. Deformed shape of the lap shear joint obtained using a geometrically nonlinear analysis.

The manner in which the total strain energy release rate G_T varies with F^2 (the square of the applied load F) is shown in Figure 6. Results for both a linear and a geometrically nonlinear analysis are shown. For perspective, the bounds for the two failure modes – fracture of the adhesive and yield of the strap – are also shown. The value of F^2 corresponding to yield of the strap is given by $(t_1\ \sigma_{yield})^2$. A discussion of the results from the linear and nonlinear analyses is presented below.

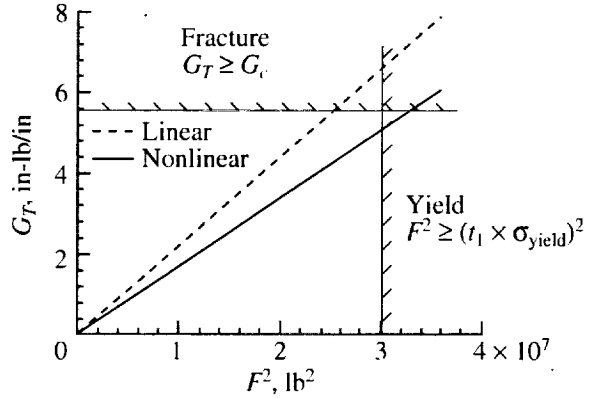

Figure 6. Total strain energy release rate G_T as a function of the square of the applied load. Failure bounds are also shown.

Linear analysis. The forces and displacements X', Y', u', and v' on the right sides of equations (3) and (4) are linear with respect to the applied load F. The total strain energy release rate G_T is calculated from the sum of the products of these quantities and hence is proportional to F^2. Thus, the results shown in Figure 6 for the linear case are expected.

Nonlinear analysis. At first glance, the nonlinear analysis curve in Figure 6 appears to be a line with a slope different from the slope of the linear analysis curve. Since that is not a reasonable conclusion, further studies were undertaken to examine the nonlinear solution in detail. The results shown in Figures 7 and 8 provide the explanation.

In Figure 7, the derivative of G_T with respect to F^2 (the slope in Fig. 6) is plotted as a function of the applied load F. Note that for the linear case the derivative is a constant, while for the nonlinear case the derivative is not a constant. The derivatives for the linear case and nonlinear case are the same at $F = 0$, but the derivatives differ for other values of F. Figure 8 provides a more dramatic contrast between the linear and nonlinear analyses. In this figure, the second derivative of G_T with respect to F^2 is plotted as a function of the applied load F. For the linear case, the second derivative is zero for all values of the load F. For the nonlinear case, the second derivative is relatively large near $F = 0$, then drops by three orders of magnitude near $F = 2000$ lb. The computational techniques used for calculating derivatives of G_T are discussed in Appendix C.

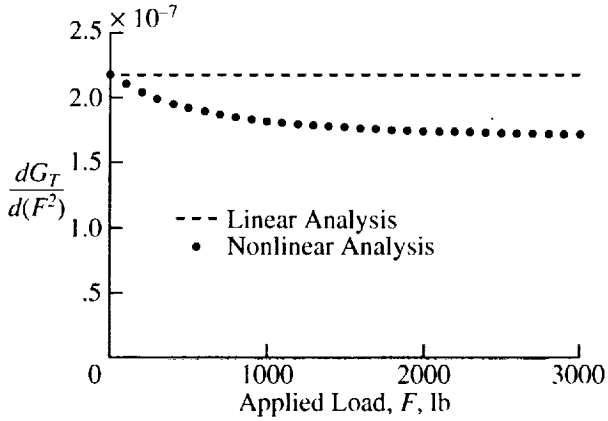

Figure 7. Derivative of G_T with respect to F^2.

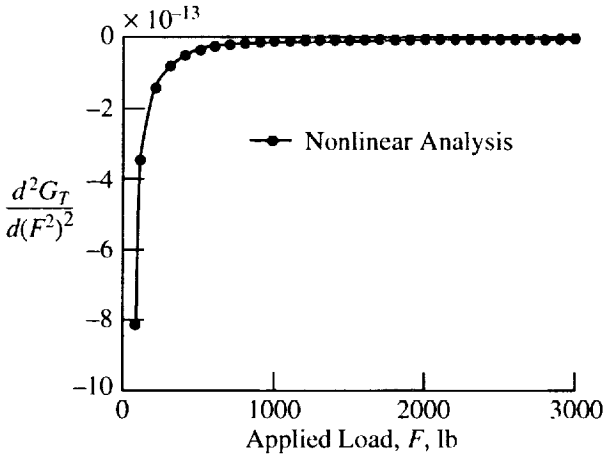

Figure 8. Second derivative of G_T with respect to F^2.

Based on the results presented in Figures 7 and 8, the nonlinear analysis curve in Figure 6 can be interpreted as follows. At $F = 0$ the slope of the nonlinear analysis curve is equal to the slope of the line for the linear solution. For values of F between zero and 2000 lb, the slope of the curve becomes smaller as the joint straightens and stiffens. The nonlinear analysis accounts for that straightening and stiffening. During straightening, G_T is not linear with respect to F^2. For values of F greater than about 3000 lb, G_T is nearly linear in F^2 with a slope that is smaller than that calculated from the linear analysis. In summary, the geometrically nonlinear analysis accounts for the joint rotation, straightening, and stiffening, while the linear analysis does not account for these phenomena. Because of the scale, the progress of the rotation, straightening, and stiffening cannot be seen in Figure 6, but the changes can be seen clearly in Figures 7 and 8.

Analysis with Uncertainties

Two distinctly different approaches for treating uncertainties are used – probabilistic and possibilistic. The effects of a geometrically nonlinear analysis and the effects of two failure modes – fracture of the adhesive and yield of the strap – are also considered. First, the convergence for a Monte Carlo simulation and a technique for greatly reducing computational effort are presented. Then, results are presented for various combinations of probabilistic and possibilistic analysis, linear and nonlinear analysis, and fracture and yield failure modes. (The headings for each of these sections have the following format: method(s) for handling the uncertainties, failure mode(s), type(s) of analysis.) Finally, probabilistic and possibilistic results are presented for a nonlinear analysis with a combination of both failure modes.

Convergence and Fracture Failure. The primary method that was used to study the effect of uncertainties was Monte Carlo simulation (MCS). Convergence of the Monte Carlo calculations was evaluated using 100, 1000, and 5000 trials and by comparing results from a Monte Carlo simulation with results from a first order reliability method (FORM). Results for 100, 1000, and 5000 trials are given in Table 2. Results are shown for both linear and nonlinear finite element analyses. In Table 2, the applied load used in the linear analysis was 5000 lb; for the nonlinear analysis the applied load was 6000 lb. (The loads in Table 2 are different for the linear and nonlinear analyses because the objectives of the analysis are to evaluate convergence in the center portion of each curve.) Based on these results, MCS with 5000 trials was considered to be adequate for the studies presented in this paper. Note that the objective was to obtain convergence in the center portion of each curve. If the emphasis were on an accurate representation of data in the tails, a larger number of trials would have been required.

Probabilistic, Fracture, Linear and Nonlinear. As previously mentioned, for the linear case the total strain energy release rate G_T varies linearly with respect to F^2. That is,

$$G_T = kF^2 \tag{6}$$

where k is a constant. Also, for the nonlinear case, G_T is nearly linear in F^2 for large values of F. This fact can be used to significantly reduce the computational resources required to produce curves such as those shown in Figure 9. In this figure, the probability of failure from fracture of the adhesive is plotted as a function of the applied load F for both a linear and a nonlinear analysis. Each curve was obtained using scaling of individual trials in a Monte Carlo simulation (n = 5000) that was carried out at a single value of the load F. The details of the scaling technique are presented in Appendix A. For the linear curve, the single value of the load F was 5000 lb; for the nonlinear curve, the single value of the load F was 6000 lb. Results obtained using FORM are included in this

Table 2. Convergence study of Monte Carlo simulation

Analysis Type	Load, lb	Probability of Failure by Fracture of Adhesive			
		Monte Carlo Simulation			FORM
		n=100	n=1000	n=5000	
Linear	5000	0.515	0.511	0.483	0.483
Nonlinear	6000	0.772	0.763	0.764	0.756

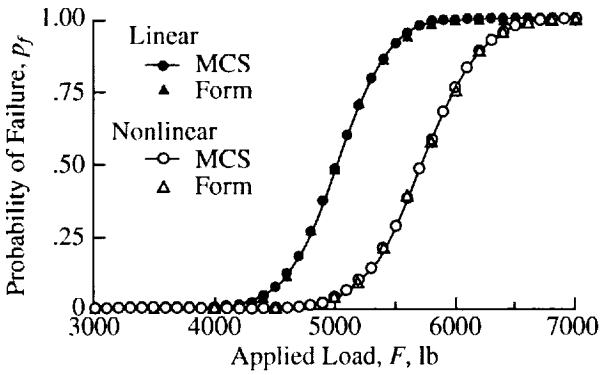

Figure 9. Probability of failure by fracture of the adhesive.

figure to confirm the accuracy of the scaling technique. Excellent agreement is obtained between the two sets of results.

Possibilistic and Probabilistic, Fracture, Linear. Figure 10 shows the possibility and probability of failure of the joint by fracture of the adhesive for a linear finite element analysis. Here and elsewhere in this paper, for a given load the possibility of failure is always greater than the probability of failure. Also note that, for this case, the possibility of failure is 1.00 when the probability of failure (p_f) is 0.50. The probability of failure p_f reaches 0.50 when the load F is 5015 lb. In the next section, this value is compared with the value obtained using a nonlinear analysis.

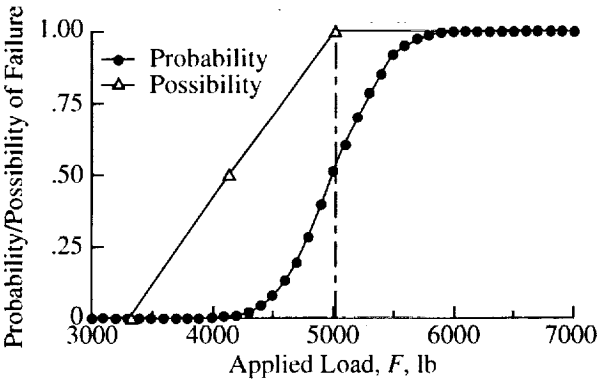

Figure 10. Possibility and probability of failure by fracture of the adhesive for a linear analysis.

Possibilistic and Probabilistic, Fracture, Linear and Nonlinear. Figure 11 shows the possibility and probability of failure of the joint caused by fracture of the adhesive using both linear and nonlinear finite element analyses. Compared with the curves for the linear analysis, the curves for the nonlinear analysis are

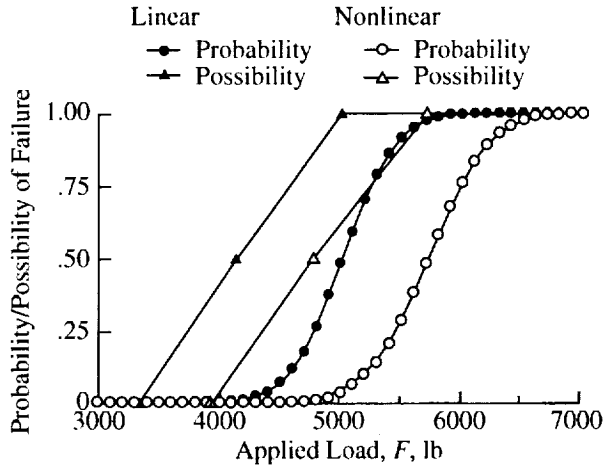

Figure 11. Possibility and probability of failure caused by fracture of the adhesive for both a linear and a nonlinear analysis.

shifted to the right. For a nonlinear analysis with p_f = 0.50, the load F is 5709 lb. Recall from the previous section that the linear analysis predicts a value of 5015 lb. According to these results and the results presented in Figure 6, a nonlinear analysis predicts that the joint can carry more load than a linear analysis – i.e., a linear analysis is more conservative. Further studies carried out in this paper are based on a nonlinear finite element analysis.

Possibilistic and Probabilistic, Material Strength. Figure 12 shows the possibility and probability of failure of the joint by material strength failure of the strap (stress σ_x greater than yield stress σ_{yield}). These results are based on equation (5) and do not require a finite element analysis. For p_f = 0.50, the value of the load F is 5500 lb, which is less than the value of

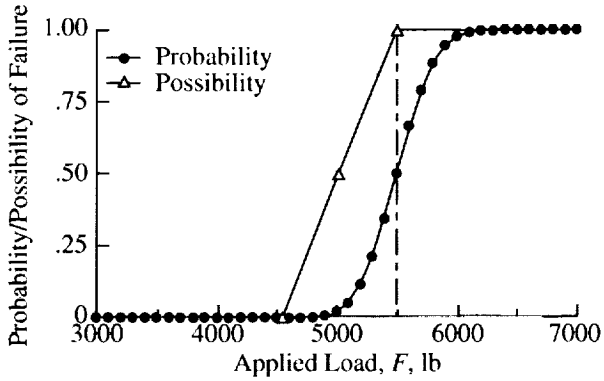

Figure 12. Possibility and probability of material strength failure of the strap.

5709 lb for the nonlinear fracture failure mode given in the previous section. The results shown in figures 10 – 12 are confirmed in figure 6 which shows that, for a nonlinear analysis with mean values of the uncertain parameters, material strength failure occurs at a lower load than fracture failure; for a linear analysis with mean values of the uncertain parameters, fracture occurs at a lower load than material strength failure.

Possibilistic, Fracture and Material Strength, Nonlinear. Figure 13 shows the possibility of failure of the joint by fracture of the adhesive (solid line) and by material strength failure of the strap (dashed line). The possibilistic failure envelope that considers both failure modes is the maximum of the possibilities of the two failure modes. (In the general case, the possibility

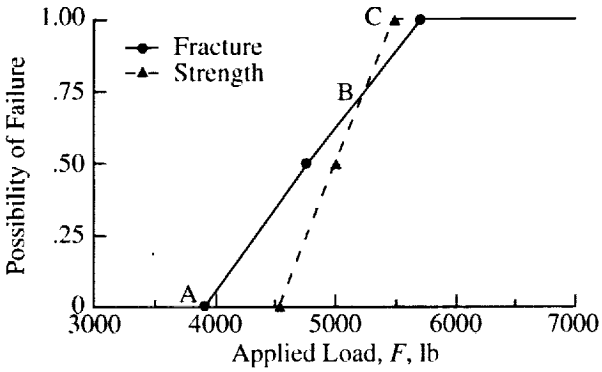

Figure 13. Possibility of failure by material strength and by fracture of the adhesive, plotted individually.

of failure is the maximum of the possibilities of all the failure modes.) In this case, the possibilistic curve that considers both failure modes starts at $\alpha = 0$ (point A) with the fracture possibilistic curve – the solid line. It follows that line up until the line crosses the strength possibilistic curve – the dashed line – at about $\alpha = 0.75$ (point B). There, the possibilistic curve that considers both failure modes shifts to the strength possibilistic curve (line BC) because, for that value of the applied load F, failure by material strength of the strap has a higher possibility than failure by fracture of the adhesive. In a possibilistic approach for handling uncertainty, if a failure mode does not have the maximum possibility for some value of the applied load, it has no effect on the possibility of failure. In contrast, in a probabilistic approach for handling uncertainty, secondary failure modes do affect the probability of failure, as discussed below.

Probabilistic, Fracture and Material Strength, Nonlinear. Figure 14 shows the probability of failure of the joint by fracture of the adhesive and by material strength failure of the strap. Three curves are shown. The first curve (filled circular symbols) is for failure of the joint by fracture of the adhesive. The second curve (filled triangular symbols) is for material strength. The third curve (open square symbols) is for either of the two failure modes or both modes – i.e., the third curve is the union of the two failure events. In the probabilistic approach for calculating the probability of failure caused by a combination of the two failure modes, both failure modes have an effect on the probability of failure, not just the more critical mode. This phenomenon can be seen in Figure 14, where the third curve is to the left of either of the two curves for the individual failure modes – i.e., the third curve indicates a higher probability of failure than either of the other two curves.

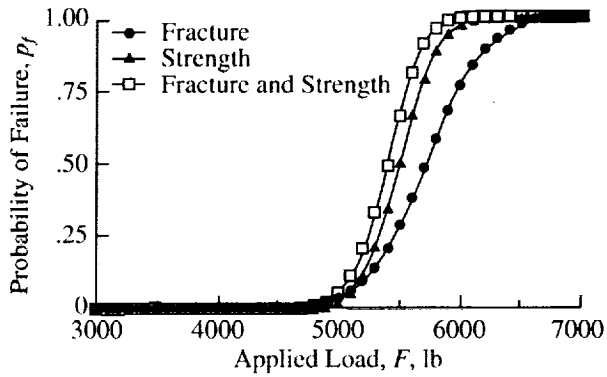

Figure 14. Probability of failure by material strength and fracture, plotted individually and in combination.

The effect of two failure modes on the probability of failure is indicated mathematically as

$$p_f(X \cup Y) = p_f(X) + p_f(Y) - p_f(X \cap Y) \qquad (7)$$

where X indicates failure by the first failure mode and Y indicates failure by the second failure mode. Finally, if there were additional failure modes, the curve that accounts for all modes would shift further to the left. That is, for a given load, that curve would indicate a higher probability of failure than the curves for any of the individual failure modes.

Probabilistic and Possibilistic, Fracture and Material Strength, Nonlinear. The results of the study are summarized in Figure 15, which shows the possibility and probability of failure of the joint by fracture of the adhesive and by material strength failure of the strap. Both curves are for a geometrically nonlinear analysis. The possibilistic curve shows the change in slope where the maximum possibility shifts from fracture of the adhesive to material strength failure of the strap. The possibility of failure becomes 1.0 at a load F of 5500 lb. The probability of failure at that load is 0.66. (In previous calculations presented in this paper, the possibility of failure becomes 1.0 when the probability of failure is 0.50. The combination of two failure modes causes that pattern to change.) The probability of failure is 0.50 at a load F of 5405 lb. For all values of the load F, the possibility of failure is greater than the probability of failure.

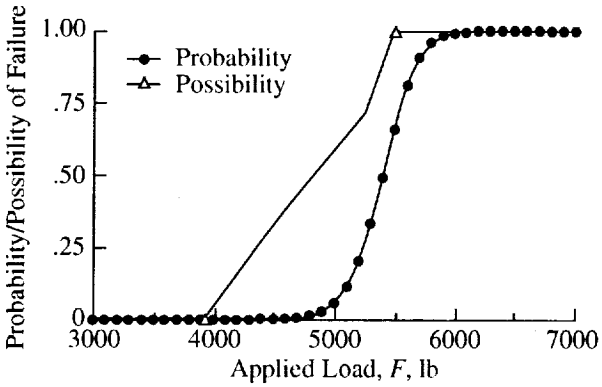

Figure 15. Possibility and probability of failure by combined material strength and fracture.

Discussion of Probabilistic and Possibilistic Methods

Based on the discussions in the previous three sections, the following contrasts can be drawn between probabilistic and possibilistic methods. Suppose a structure has many failure modes any of which can cause the structure to fail – i.e., the structure is a series system. (The single lap shear joint with two failure modes is an example of a series system.) In a probabilistic analysis the probability of failure increases with each failure mode considered. In contrast, in a possibilistic analysis the possibility of failure increases only if a failure mode is introduced that has a larger possibility of failure than any other failure mode. For example, suppose that the structure is a chain of identical links. The probability of failure increases with increasing chain length. The possibility of failure remains the same regardless of chain length. As a result, for multiple failure modes a possibilistic analysis may become unconservative.

Using the same reasoning, a possibilistic approach could exhibit unexpected behavior for a structure with redundancies – i.e., a parallel system. The probability of failure of the structural system is reduced as the redundancy is increased. In contrast, the possibility of failure of the structural system is equal to the possibility of failure of the component having the largest possibility of failure – regardless of the number of redundancies. As a result, for redundant systems a possibilistic approach is conservative. An excellent in-depth discussion of probabilistic versus possibilistic methods is presented in Reference 11.

Possibilistic approaches for treating uncertainties may be viable for early design. But it is not clear that possibilistic approaches are superior to probabilistic approaches for early design. For example, whereas the number of function evaluations for a possibilistic analysis may be small compared with a Monte Carlo simulation, the number of function evaluations may be comparable to that required by some probabilistic methods such as FORM. These probabilistic methods can provide more information than possibilistic methods. Furthermore, even though the possibility of failure was always greater than the probability of failure for the bonded joint example with two failure modes, the assumption that possibilistic design is conservative is not a valid assumption when there are many failure modes. In many cases, the choice of methods depends upon the availability of data. Finally, the choice of methods depends upon the designer – how familiar he is with the characteristics of both the methods and the design problem.

Concluding Remarks

This paper has explored the effects of configurational and material uncertainties on the strength of a single lap shear joint. Finite element analyses were used to study the joint. Both probabilistic and possibilistic approaches for accounting for uncertainties were studied, and results from the two approaches are compared. The effects of a geometrically nonlinear analysis and two failure modes are presented. A computational technique for speeding the calculation of the probability of fracture failure at various loads is presented.

Geometrically nonlinear analyses are essential for accurately predicting the response of the single lap shear joint and its fracture failure mode. The joint

begins to straighten out and stiffen at a low load. This phenomenon can be predicted with a geometrically nonlinear analysis, but it cannot be predicted with a linear analysis. A geometrically nonlinear analysis predicts that the joint can carry more load than is predicted by a linear analysis.

For a linear analysis, the strain energy release rates are proportional to the square of the applied load. For a geometrically nonlinear analysis, the strain energy release rates are almost proportional to the square of the applied load for large values of the applied load. These characteristics make it possible to employ scaling to substantially reduce computational effort.

Possibilistic approaches for treating uncertainties may be viable for early design. But it is not clear that possibilistic approaches are superior to probabilistic approaches for early design.

References

1. Brussat, T. R., Chiu, S. T., and Mostvoy, S., "Fracture Mechanics for Structural Adhesive Bonds – Final Report," AFML-TR-77-163, Air Force Materials Laboratory, Wright Patterson Air Force Base, Dayton, OH, 1977
2. Johnson, W. S., (1987), "Stress Analysis of the Cracked-Lap-shear Specimen: An ASTM Round-Robin," *J. of Testing and Evaluation,* Vol. 15, pp. 303-324.
3. Lai, Y.-H., Rakestra, M. D., and Dillard, D. A., (1996), "The Cracked Lap Shear Specimen Revisited - A Closed Form Solution," *Int. J. of Solids and Structures*, Vol. 33, No. 12, pp. 1725-1743.
4. Tong, L., and Steven, G. P., (1999), "Analysis and Design of Structural Bonded Joints," Kluwer Academic Publishers, Boston/Dordrecht/London.
5. Mall, S., and Johnson, W. S. (1985), "Characterization of Mode I and Mixed Mode Failure of Adhesive Bonds Between Composite Adherends," NASA Technical Memorandum 86355.
6. ABAQUS Users Manual, Version 5.8, (1998), Hibbitt, Karlsson, and Sorensen, Inc., 1080 Main Street, Pawtucket, RI 02860-4847.
7. Melchers, R. E., (1999), "Structural Reliability, Analysis and Prediction," Chichester; New York : John Wiley
8. Elishakoff, Isaac, (1999), "Probabilistic Theory of Structures," Second Edition, Dover Publications, Inc., Mineola, NY.
9. Cesare, Mark, A. and Sues, Robert, H., (1999), " ProFES Probabilistic Finite Element System-Bringing Probabilistic Mechanics to the Desktop", Proceedings of 40th AIAA/ASME/ASCE/AHS/ ASC Structures, Structural Dynamics, and Materials Conference, April 12-15, 1999, St. Louis, MO, Paper NO. AIAA-99-1607, 1999.
10. Dong, W., and Shah, H.C., (1987), "Vertex Method for Computing Functions of Fuzzy Variables," Fuzzy Sets and Systems, 24, pp. 65-78.
11. Nikolaidis, Efstratios; Cudney, Harley; Chen, Sophie; Haftka, Raphael T.; and Rosca, Raluca, (1999), "Comparison of Probabilistic and Possibility Theory-Based Methods for Design Against Catastrophic Failure Under Uncertainty," Proceedings of the 1999 ASME Design Engineering Technical Conferences, 11th International Conference on Design Theory and Methodology, Sept. 12-15, 1999, Las Vegas, Nevada. Available as DETC99/DTM-8758.
12. Rybicki, E. F., and Kanninen, M. F., (1977), "A Finite Element Calculation of Stress-Intensity Factors By A Modified Crack Closure Integral," Engineering Fracture Mechanics, Vol. 9, pp. 931-938.
13. Raju, I. S., (1987), "Calculation of Strain-Energy Release Rates with Higher Order and Singular Finite Elements," Engineering Fracture Mechanics, Vol. 28, No. 3. pp. 251-274.
14. Ramamurthy, T. S., Krishnamurthy, T., Narayana, K. B., Vijayakumar, K., and Dattaguru, B., (1986), "Modified Crack Closure Integral Methods With Quarter Point Elements," Mech. Res. Commun.., Vol. 13, pp. 179-286.
15. Smith, S.A., and Raju, I.S., "Evaluation of Stress-Intensity Factors Using General Finite-Element Models," Fatigue and Fracture Mechanics: Twenty-Ninth Volume, ASTM STP 1332, T.L. Pantonin, and S.D. Sheppards, Eds., American Society for Testing and Materials, West Conshohocken, PA, 1999, pp. 176-199.
16. Krueger, R., Minguet, P., and O'Brien, T., (2000), "A Method for Calculating Strain Energy Release Rates in Preliminary Design of Composite Skin/Stringer Debonding Under Multiaxial Loading," Composite Structures: Theory and Practice, ASTM STP 1383, P. Grant and C. Q. Rousseau, Eds., American Society for Testing and Materials, West Conshohocken, PA, 2000, pp. 105-128.
17. Reeder, J. R., (1992), "An Evaluation of Mixed-Mode Delamination Failure Criteria," NASA-TM-104210.
18. Reeder, J. R., (1993), "Bilinear Fracture Criterion for Mixed-Mode Delamination," *Composite Materials: Testing and Design-11th Volume*, ASTM STP 1206, American Society for Testing and Materials, West Conshohocken, PA, 1993, p. 303-322. Also available as NASA-TM-111543.

Appendix A. Monte Carlo Simulation and Scaling of Strain Energy Release Rate

Monte Carlo simulation involves carrying out a large number of numerical experiments, or trials, with random values of the quantities that are selected to be random variables. In the trials, the randomness of each random variable is guided by the statistics specified for that variable – e.g., type of distribution, mean, and standard deviation.

In the present study, for each Monte Carlo trial a statistically independent configuration of the lap joint is created from the random values of the input variables. A finite-element model is developed for that configuration and a finite element analysis is performed to calculate the total strain energy release rate G_T.

In a given trial, if the calculated value of G_T exceeds the experimentally determined critical value G_C, the configuration is considered to have "failed". For example, if the total number of trials in a simulation is 5000 and if there are 3000 failures, then the probability of failure is 0.6 for this specific load.

Suppose the first Monte Carlo simulation is conducted with $F = F_0$. In the general case, in order to obtain the probability of failure for a different load F_1, the Monte Carlo simulation would have to be repeated for the new load value. However, by utilizing the fact that G_T is linear with respect to F^2, it is possible to substantially reduce the computational effort. For each trial, the value of G_T, for all loads $F = F_1$, can be calculated by scaling the value of G_T calculated for $F = F_0$. The scaling is carried out in the following way:

$$G_T\big|_{F=F_1} = \left(\frac{F_1}{F_0}\right)^2 G_T\big|_{F=F_0} \qquad \text{(A1)}$$

The value of G_T obtained through scaling for each trial is compared with the corresponding value of G_C. The number of failures are counted to calculate the probability of failure for the current load, $F = F_1$. Hence, it is sufficient to perform the Monte Carlo simulation only once for an arbitrary load. The probability of failure for any other load can be calculated by scaling G_T for each specific trial.

In the present study, scaling of G_T is used to calculate the probability of failure for both linear and nonlinear finite element analyses.

Appendix B. Calculating with Membership Functions

Let α be a parameter that indicates the possibility of an uncertain quantity taking on a given value. The parameter α takes on values between zero and one. A value of zero indicates no possibility, while a value of one indicates maximum possibility. A membership function describes the relationship between α and the possible values of the uncertain quantities. An example of a membership function is shown in Figure 3. In a possibilistic analysis, each of the uncertain quantities that contribute to the response is defined in terms of a membership function. The objective of the possibilistic analysis is to determine the corresponding membership function of the response quantities. The membership functions of the response quantities can then be compared with the membership functions for the allowable responses to determine the possibility of failure.

A simple example is used to illustrate how to perform calculations using membership functions. Consider the cantilever beam shown in Figure B1. The tip deflection δ is given by

$$\delta = \frac{PL^3}{3EI} \qquad \text{(B1)}$$

where P is the load at the tip, L is the length, E is Young's modulus, and I is the moment of inertia. Assume that L and I are uncertain quantities with membership functions similar to that shown in Figure B2. The vertical scale is the possibility, denoted α, which varies from zero to one. The values of E and P are taken to be 10^7 psi and 100 lb, respectively.

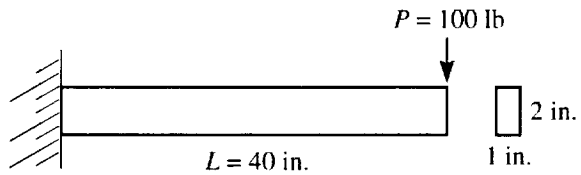

Figure B1. Cantilever beam example.

The membership functions for L and I are isosceles triangles with upper and lower bounds (UB, LB) shown in Table B1. The bounds are for $\alpha = 0.0$, 0.5, and 1.0. The objective is to obtain an estimate of the uncertainty in δ by calculating its membership function.

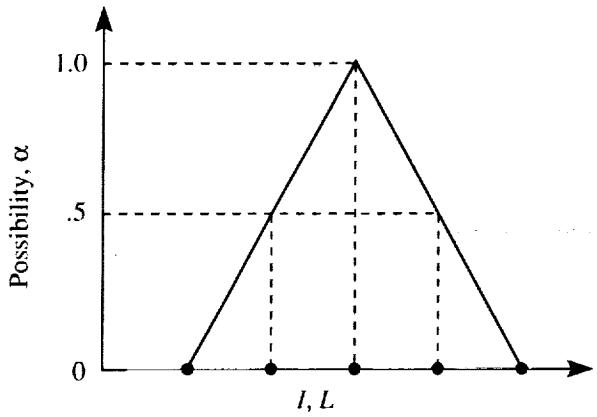

Figure B2. Example membership function for moment of inertia I and length L of cantilever beam example. (Filled circles indicate bounds on I and L corresponding to α = 0.0, 0.5, and 1.0.).

To obtain the upper and lower bounds for δ at $\alpha = 0.0$, calculate δ for various combinations of L and I within their $\alpha = 0.0$ bounds and select the largest and smallest values. That is, calculate δ for several combinations of L and I in the ranges $39.8 \le L \le 40.2$ and $0.64583 \le I \le 0.68750$. To obtain the upper and lower bounds for δ at $\alpha = 0.5$, calculate δ for various combinations of L and I within their $\alpha = 0.5$ bounds and select the largest and smallest values. That is, calculate δ for several combinations of L and I in the ranges $39.9 \le L \le 40.1$ and $0.65625 \le I \le 0.67708$. The same approach is used for other values of α. To obtain the most likely value of δ, which is the value corresponding to $\alpha = 1.0$, use the most likely values of L and I, 40.0 and 0.66667, respectively.

For this simple example it is easy to select the values of L and I that give the upper and lower bounds on δ. The upper bound on δ is given by a combination of the upper bound on L and the lower bound on I. The lower bound on δ is given by a combination of the lower bound on L and the upper bound on I.

In general, to calculate the upper and lower bounds on a response quantity at a given value of α it is necessary to use several combinations of values of the independent variables at that same value of α. These values include both the bounds and values between the bounds. It cannot be assumed that bounds on the response quantities can be identified by considering only the bounds on the independent variables.

Appendix C. Computational Techniques Used for Calculating Derivatives of G_T

The data for Figures 7 and 8 were obtained using a combination of chain rule differentiation and finite difference approximations. The chain rule differentiation provided expressions containing derivatives of G_T with respect to F rather than F^2. That change was made because the values of G_T were calculated at equal increments in F (100 lb increments) rather than equal increments in F^2. As a result, multipoint finite difference approximations could be more accurate for derivatives with respect to F than for derivatives with respect to F^2.

For example, for Figure 8, chain rule differentiation provides the following expression

$$\frac{d^2G_T}{d(F^2)^2} = \frac{1}{4F^2}\frac{d^2G_T}{dF^2} - \frac{1}{4F^3}\frac{dG_T}{dF} \qquad \text{(C1)}$$

The values of the derivatives on the right hand side in equation (C1) were calculated using 4- and 5-point finite difference approximations. The value of $\frac{d^2G_T}{d(F^2)^2}$ at $F \approx 70$ lb was calculated with a 2-point central difference formula. The computational technique described above was most valuable in calculating $\frac{d^2G_T}{d(F^2)^2}$ for small values of F where that derivative is changing rapidly.

Table B1. Assumed bounds on independent variables I and L and corresponding calculated bounds for tip deflection of cantilever beam example

α	I in.^{4}		L in.		δ in.	
	LB	UB	LB	UB	LB	UB
0.0	0.64583	0.68750	39.800	40.200	0.30567	0.33530
0.5	0.65625	0.67708	39.900	40.100	0.31272	0.32752
1.0	0.66667	0.66667	40.000	40.000	0.32000	0.32000